Capacity of a Binary Droplet-Based Microfluidic Channel with Memory and Anticipation for Flow-Induced Molecular Communications

L. Galluccio, A. Lombardo, G. Morabito, S. Palazzo, C. Panarello, G. Schembra

***Abstract*—Flow-induced Molecular Communications are a promising communication paradigm based on the exchange of molecule concentrations in a continuous fluid, guided and directed through microfluidic pipes. An emerging approach to implement this type of communications is based on discrete (or droplet-based) microfluidics. It exploits the idea to represent binary information by encapsulating the signaling molecules inside droplets which are dispersed in an immiscible fluid and delivered, through micro pipes, to the destination. The objective of this work is to study a binary droplet-based microfluidic system for flow-induced molecular communications from an information theoretical perspective. To this end, we first show that the binary discrete microfluidic channel is characterized by memory and anticipation. Accordingly, we provide a mathematical model based on a finite-state Markov chain. Finally, we evaluate the capacity of the binary droplet-based microfluidic channel.**

***Index Terms*—Flow-induced molecular communications, Droplet-based microfluidics, channel capacity, channel with memory and anticipation, Markov models.**

I. Introduction

MOLECULAR communications have emerged as an alternative approach to communicate in scenarios where data transmission through electromagnetic waves is limited by several constraints [1]. Taking inspiration from biological communication processes, small amounts of matter (e.g. molecules) are used to encode messages and propagate signals for communications at both nano- and micro-scales [25], [3].

One of the most widely considered mechanisms for molecular communications is based on the so-called *diffusion-based* approach [28], where molecules, subject to the Brownian motion, spread their concentration throughout the available medium. However, when diffusion in free space is employed as the mass transport phenomenon, communications suffer from high levels of attenuation and delay. In order to overcome these shortcomings, an emerging approach, called Flow-induced Molecular Communications, has been proposed [4], [26]. It relies on the *flow-based molecular transport*, i.e., the molecules encoding a message are dispersed in a continuous medium, flowing inside micro pipes which guide and direct the molecules, thus increasing the efficiency of the propagation mechanism.

Micro pipes are today used in relevant microfluidic systems such as Labs-on-a-Chip (LoCs) [29]. The mainstream approach to microfluidics in general, and to flow-induced molecular communications in particular, has been based so far on the manipulation of continuous flows through micro pipes. However, in recent years promising opportunities and applications have been identified which rely on the introduction of an emerging approach named droplet-based microfluidics [34], [35] where a sequence of droplets or bubbles (called *dispersed phase*) are dispersed into another fluid (called *continuous phase*), immiscible with them. Thus, it is possible to bind molecules inside droplets which can be controlled independently of each others, so paving the way to unconventional communications and computing facilities using droplets in microfluidic systems [31], [18].

The binary discrete microfluidic channel we study in this paper is based on discrete (i.e. droplet-based) microfluidics, and exploits the idea to represent binary information by encapsulating the signaling molecules inside droplets delivered, through micro pipes, to the destination. The discrete approach to molecular communications through microfluidics has been investigated in [13], [18], [10]. However, in order to evaluate the molecular communications performance of a discrete microfluidic system, and exploit its potential practical applications, a binary discrete microfluidic channel model and a theoretical analysis of its information capacity are necessary.

From an information theoretical perspective, some researchers have approached the study of the capacity of diffusion-based molecular communications channels [16], [24]. In particular, molecular communications in continuous microfluidics have been investigated in [5], [26], [7], [8], and the related capacity analysis is presented in [6]. However, so far there is no work on analytical models and information capacity analysis of a discrete microfluidic channel for molecular communications, although droplet-based communications in microfluidic devices have been proposed in [13], [14].

Therefore, in this work a droplet-based microfluidic system for molecular communications, where binary information is encoded by encapsulating signaling molecules in a droplet, is considered and analyzed from an information-theoretic point of view. Original contributions of this work are manifold. First, we analyze possible causes of errors and derive a *noise statistical characterization* for the microfluidic channel, based on experimental measurements on linear micro pipes, for several sections and flow rates.

Then, we introduce a *mathematical model* of the binary discrete microfluidic channel. Specifically, we show that in relevant cases the microfluidic channels are characterized by *memory and anticipation*, i.e., for a given current input, the

Authors are with the Department of Electrical, Electronic and Computer Engineering (DIEEI), University of Catania, Italy. e-mail:{name.surname}@dieei.unict.it

current output is statistically depending on the previous history as well as on future inputs. The uncommon assumption of anticipatory behavior for the system under study is not related to the use of some prediction mechanism of the future symbols, as one might legitimately think. It is, instead, related to the presence of phenomenons involving more than one symbol in the spatial domain [30], so that the output symbol resulting from the spatial interference between a droplet and the following (that is the *future*) one may anticipate information about the symbol associated to the latter droplet. In this paper, channel memory and anticipation are managed by enclosing both past and future input symbols in the channel state, as typically done in the literature on channels with memory [21], [27].

Finally, we apply the above model to derive an *information capacity analysis* of the microfluidic channel. Note that in information theory the capacity of channels with memory and anticipation is, as it is said in mathematics, not *well-defined* in general. In fact, different definitions of such capacity are possible leading to different interpretations and numerical values [17], [24]. Moreover, even if in some specific cases such capacity is well-defined, calculation of the mutual information is usually intractable [2], [21]. In order to evaluate the information capacity of the droplet-based microfluidic channel, in this paper we verify that in our case memory and anticipation are finite, that is, they are related to a finite number of slots. This occurrence allows us to state that the information capacity is well-defined for the channel under study [24], and to provide a closed-form expression of the mutual information rate.

The paper is organized as follows. The addressed droplet-based microfluidic system for molecular communications is described in Section II. In Section III, we statistically characterize the noise of the microfluidic channel. The mathematical model is introduced and applied to derive the channel capacity in Section IV and V, respectively. Numerical results are introduced in Section VI. Finally, in Section VII, some conclusions are drawn.

II. System description

Flow-induced Molecular Communications exploit the possibility of using small amounts of matter (i.e. signaling molecules) to encode messages and propagate them through a fluid medium inside microfluidic pipes[1]. More specifically, in this work, we focus on Flow-induced Molecular Communications through droplet-based microfluidics. The schematic diagram of a droplet-based microfluidic system is shown in Fig. 1. The *Source/Encoder* produces the message to be sent to the destination in the form of binary string. Then the *Molecular Digital Baseband Modulator* converts the digital bit stream into a molecule concentration inside droplets (the signal), that can be physically transmitted across a *Droplet-based Microfluidic Channel*. The latter consists of a linear microfluidic pipe[2], through which the train of droplets (dispersed phase) generated by the molecular digital baseband modulator flows, dispersed in another fluid (continuous phase) immiscible with the droplets, to the receiver. Here the *Molecular Digital Baseband Demodulator* is used to receive the incoming droplets and to convert the sequence of droplets into the original digital bit stream encoding the message. The *Decoder/Destination* is the recipient of the messages. In the following we will focus on the *Physical System*, composed by the Molecular Digital Baseband Modulator, the Droplet-based Microfluidic Channel and the Molecular Digital Baseband Demodulator.

According to the digital bit stream encoding the message, the Molecular Digital Baseband Modulator generates droplets of the same size, at a constant droplet rate. At regular time intervals of duration T_b, two different types of droplets are generated to encode the bits '1' and '0'. As an example, the message can be encoded in the presence or absence of the signaling molecules inside the droplets, in the different concentration of signaling molecules or in the different types of signaling molecules associated to the bits '1' or '0', respectively. Such a sequence of droplets represents the *Transmitted Molecular Signal X* in Fig. 1.

The train of droplets is transported by the continuous phase through the Droplet-based Microfluidic Channel at an average velocity v, which is assumed to be constant given that the channel is linear. However, it has been experimentally observed that the droplet instantaneous velocity varies due to a number of physical factors, including viscosity of the fluid phases, pressure fluctuations, irregularity and roughness of the microfluidic pipes [32], [20]. As a consequence the droplet inter-arrival time at a generic section of the channel, that is the time interval between the arrival at the same section of a pair of droplets, suffers variations as well. In this study, the variation of the inter-arrival time between pairs of droplets is envisioned as the noise in the microfluidic channel and may lead to communication errors, which will be analyzed in detail in Section III. We will see that such a noise may modify the sequence of droplets that reaches the receiver, so producing a *Received Molecular Signal Y* different from the transmitted one.

Once the droplets reach the receiver, the Molecular Digital Baseband Demodulator is used to perform demodulation operations on the Received Molecular Signal Y. More specifically, detectors for the chemical content of the droplets have to be used to reveal the message. As an example, chemi- or bio-luminescence can be used to decode the message by revealing the composition of droplets through their combination with reagents that activate the luminescence phenomenon, as illustrated in Fig. 2. In this way, a train of luminescent and non-luminescent droplets, or a train of luminescent droplets of different colors, may be obtained at the receiver where the message can be revealed through the use of an appropriate sensing device. Finally, the revealed message can be converted to a digital bit stream.

[1]Note that in the microfluidic literature the term *channel* is used instead of *pipe*. In this paper, to avoid confusion, we use the term *channel* with the same meaning used in the information theory literature, whereas the term *pipe* is used to identify the physical system where droplets flow.

[2]The capacity analysis of a non-linear microfluidic channel, that is a micro pipe where branches, splitting or section variations are present, is out of the scope of this paper.

This article has been accepted for publication in a future issue of this journal, but has not been fully edited. Content may change prior to final publication. Citation information: DOI 10.1109/TCOMM.2017.2755649, IEEE Transactions on Communications

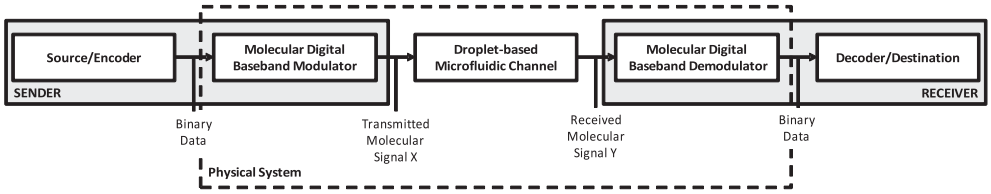

Fig. 1. Information-theoretic scheme of a droplet-based microfluidic system for molecular communications

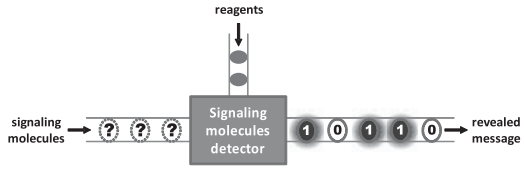

Fig. 2. Example of chemi- or bio-luminescence detection

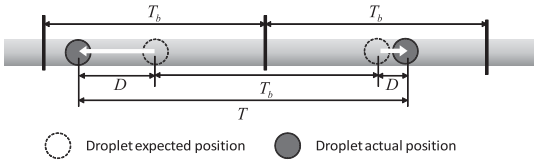

Fig. 3. Distance between droplets

(a) Irregularity and roughness in the pipe

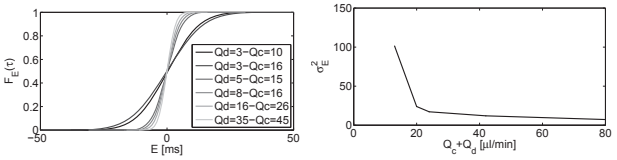

(b) Cdf of E (c) Variance of E

Fig. 4. Experimental measurements

III. Noise Characterization

The system we are considering in this paper is designed to send, and then receive, one droplet in each time slot of duration T_b, and therefore synchronization between the droplet reception and the detection operations is required. However, due to a large number of physical factors, including fluid viscosity, pressure fluctuations, irregularity and roughness of the microfluidic channels, the droplet inter-arrival time at the receiver suffers variations that may cause loss of synchronization at the receiver side [32], [20]. Moreover, when the inter-arrival time between two droplets decreases, obviously the distance decreases as well, and if the latter becomes lower than a critical value Δ_C (which depends on the radius of the channel, velocity of motion, surfactant concentration and type of surface forces, among other physical factors [12]), droplets interact with each others. As a result of such interactions, coalescence (i.e. fusion) of droplets may occur, i.e. two droplets undesirably join into a single one. In this case, the information associated with the two original droplets may be lost and the message corrupted.

For these reasons, any variation of the inter-arrival time between consecutive droplets represents a noise in the microfluidic channel connecting a droplet-based information source to a receiver. Other causes of errors, such as obstruction of the microfluidic channels as well as deformation and breakup of the droplets, are possible. However, obstructions are mostly due to flaws in the fabrication of the microfluidic chip and dirt left in the channel by the utilized fluids, therefore they should and, actually, can be avoided. Furthermore, obstructions would result in a failure of the channel rather than in decrease of the capacity. As regards droplet deformation and breakup, they occur when the flow rates are not consistent with the characteristics of the fluids and the geometry of the system, i.e., when the system is working outside its *safe operating region*, which can be *a priori* determined as discussed in the large body of related literature (see [22] for a review on the topic). Let us stress that, for all these reasons, the above causes of errors, although possible in general, are very unlikely, especially in a linear micro pipe without any branch or section variation, as actually is the microfluidic channel we are addressing in this paper. Therefore, we assume that the variation of the distance between consecutive droplets is the only cause of errors.

In this section, we statistically characterize the noise of the droplet-based microfluidic channel starting from experimental measurements conducted on several micro pipes with multiple sections and flow rates. In particular, we focus on the inter-arrival time variation between pairs of consecutive droplets flowing through a linear micro pipe [15]. In Fig. 4(a) we show a portion of one of the micro pipes we have used in our experiments. Such figure gives an idea of the irregularities and roughnesses characterizing a microfluidic pipe.

Let T be the inter-arrival time of two droplets at a generic section of the pipe (its value at the generation point is T_b), and let $E = T - T_b$. All the cases we have analyzed show that E can be modeled as a Gaussian random variable with average μ_E equal to zero, and variance σ_E^2 that does not depend on the distance of the observation point from the droplet generation point [13].

Let $f_E(\tau)$ be the probability density function (pdf) of E, and $F_E(\tau)$ its cumulative distribution function (cdf). Fig. 4(b) shows the cdf measured in a micro pipe with a section size of 200x400nm, for different values of the continuous and disperse flow rates, Q_c and Q_d, respectively. Fig. 4(c) shows how the variance of the above Gaussian distribution depends on the global flow rate in the micro pipe, $Q_c + Q_d$.

The experimental measurements have also shown that the

This article has been accepted for publication in a future issue of this journal, but has not been fully edited. Content may change prior to final publication. Citation information: DOI 10.1109/TCOMM.2017.2755649, IEEE Transactions on Communications

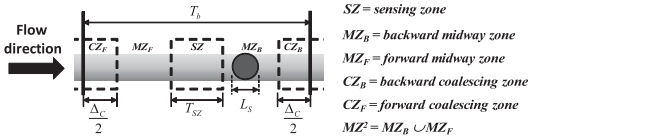

(a) Time slot zones when $T_{SZ} < T_b - \Delta_C - 2L_S$

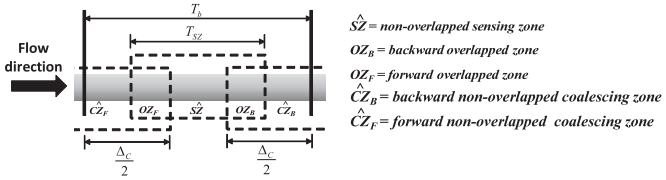

(b) Time slot zones when $T_{SZ} \geq T_b - \Delta_C - 2L_S$

Fig. 5. Graphical representation of time slot zones

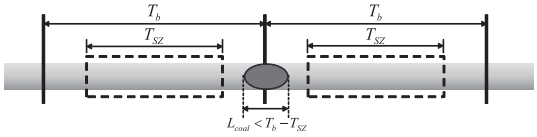

(a) Hidden coalesced droplet: $L_{coal} < T_b - T_{SZ}$

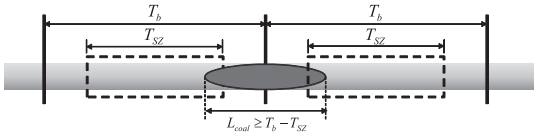

(b) Exposed coalesced droplet: $L_{coal} > T_b - T_{SZ}$

Fig. 6. Coalesced droplet

difference E can be considered as an additive noise independent from the distance T_b of the two droplets at the generation point. Consequently, the inter-arrival time, T, between two droplets, in a generic section of the microfluidic channel, can be described as a Gaussian random variable, $T = T_b + E$, whose pdf, $f_T(t)$, can be described by the mean value T_b and the variance σ_E^2.

Droplets are expected to be received in the center of the time slot to be correctly decoded. Let t_e be the expected arrival time of a generic droplet, and t_a be its actual arrival time. The difference $D = t_a - t_e$ between the actual and the expected arrival times can be described as a random variable, whose pdf, $f_D(d)$, can be easily derived from $f_E(\tau)$. In fact, let us denote the delay of two consecutive droplets with respect to their expected position as $D_1 = t_{a1} - t_{e1}$ and $D_2 = t_{a2} - t_{e2}$, respectively. Note that the difference between the expected arrival times corresponds to the time interval T_b between the generation of the two droplets, i.e. $t_{e2} - t_{e1} = T_b$. Similarly, the difference between the actual arrival times corresponds to the inter-arrival time T, i.e. $t_{a2} - t_{a1} = T$. Accordingly, it is easy to demonstrate that the difference between D_2 and D_1 is equal to E. Thus D_1 and D_2 can be described as independent random variables whose linear combination is the Gaussian random variable E. Therefore, the distribution $f_D(d)$ of D is a Gaussian function with average μ_D equal to zero and variance $\sigma_D^2 = \frac{\sigma_E^2}{2}$.

IV. Channel Model

In this section we model the droplet-based microfluidic channel. The possible input and output droplet types are represented by the random variables X and Y, respectively.

According to the specific signaling molecules dissolved in the droplet, the input random variable X takes values in a binary alphabet $\mathcal{X}$, whose elements are here referred to as A and B, i.e., $\mathcal{X} = \{A, B\}$.

In order to define the output alphabet $\mathcal{Y}$ where the output random variable Y takes values, we need to consider the types of output droplets that may be received. To this purpose let us observe that, at the input of the channel, droplets are equally spaced, whereas as droplets flow through the channel, the distance between consecutive droplets may vary as described in Section III, and droplet misplacement inside the time slot is possible. Let us denote the region around the center of a time slot within which the droplet can be detected as *sensing zone*, *SZ*, (see Fig. 5), and let T_{SZ} be its length [3]. When the droplet misplacement is such that the droplet moves outside the sensing zone, the synchronization fails and the droplet will not be detected, leaving a hole in the sequence of the received droplets. Moreover, when the distance between two droplets decreases below the critical value Δ_C, droplet coalescence may occur, so producing a new sequence with different type and number of droplets.

Therefore, when droplets move away from their expected position in the center of the time slot, two cases are possible:

- A droplet moves outside the sensing zone and does not coalesce with an adjacent one: in this case, no droplets will be detected inside the sensing zone. In order to take this event into account, the output alphabet $\mathcal{Y}$ of received symbols includes, beyond the symbols A and B of the input alphabet $\mathcal{X}$, also the symbol $\emptyset$.
- Two droplets coalesce into a single one: let L_{coal} be the length of the coalesced droplet. For worth of simplicity, we will assume that the new joined droplet is likely centered in the boundary between the two original time slots. So, depending on whether its length L_{coal} is greater or lower than the distance between two consecutive sensing zones (i.e. $L_{coal} \geq T_b - T_{SZ}$ or $L_{coal} < T_b - T_{SZ}$), respectively, several results are feasible. More specifically:
  - *Hidden coalesced droplet*: When the length L_{coal} of the coalesced droplets is smaller than the distance between the two sensing zones as in Fig. 6(a), i.e. $L_{coal} < T_b - T_{SZ}$, the coalesced droplet remains outside the sensing zones of the two time slots, and no droplets are detected for the two time slots. This case has been mapped into the output symbol $\emptyset$, which has been included in the output alphabet $\mathcal{Y}$.

[3]Note that the association of message symbols to droplets that physically move in the spatial domain, allows to describe the communication through the discrete microfluidic channel between a sender and a receiver, interchangeably in the time and spatial domains. Specifically, distances (for example, *time slot length*) and time intervals (for example, *time slot duration*) are proportional quantities, that is, their ratio is equal to the constant average velocity, v, of the continuous phase through the channel. For this reason in the paper we will interchangeably refer to *duration* and *length* without distinction. However, for the sake of consistency, their are always intended to be time interval when used in the equations.

– *Exposed coalesced droplet*: When, on the contrary, the length L_{coal} of the coalesced droplets is greater than the distance between the two sensing zones, i.e. $L_{coal} \geq T_b - T_{SZ}$, the coalesced droplet is detected in both time slots (see Fig. 6(b)). According to the types of the two coalescing droplets, different coalesced droplet types can be produced: in particular, the two coalescing droplets may be associated either to the same symbol A or B, or one droplet to the symbol A and the other one to the symbol B.
In the case both droplets are originally associated to the same symbol, each portion of the coalesced droplet detected in each sensing zone would be interpreted as a single droplet of the same type of the transmitted one, so the output symbols would be the same as the input ones. In the case the two droplets involved in the coalescence event are associated to different symbols, each portion of the coalesced droplet detected in each time slot would be different from any of the input symbols, and therefore, the two corresponding droplet types remain unidentified. To represent this case, the additional symbol U is included in the output alphabet $\mathcal{Y}$.

Therefore, depending on the length of the droplet resulting from the coalescence, two different output alphabets $\mathcal{Y}$ are defined, i.e. $\mathcal{Y} = \{A, B, \emptyset\}$ and $\mathcal{Y} = \{A, B, \emptyset, U\}$ for the cases of hidden and exposed coalesced droplets, respectively, as shown in Fig. 7. Unfortunately, the differences between the two cases are not only on the output alphabet $\mathcal{Y}$, but also on the different properties characterizing the related channel models. To give more insight into the problem, let us discuss the implications of a coalescence event in the case the length of the coalesced droplet is either greater or lower than the distance between the two sensing zones.

In the case $L_{coal} < T_b - T_{SZ}$, if a coalescence event occurs, the coalesced droplet remains hidden outside the sensing zone. In this case, the produced output symbol is $\emptyset$, regardless of the sequence of input symbols. Therefore, the channel can be modeled as a memoryless discrete channel, whose capacity calculation is given by the well known Shannon's formula [33]. In Section IV-A, we present the model of the channel in this case.

Conversely, when $L_{coal} \geq T_b - T_{SZ}$, as said so far, if two droplets coalesce in a single one, the output symbols A, B or U may be produced depending on whether the two coalescing droplets are both of type A or B, or of different types. Note that the coalescence event involves droplets associated to two different time slots; therefore, for these two time slots the output symbols depend on both the corresponding inputs (i.e. on the type of the droplet associated to the same time slot). When we focus on the second of these two time slots, the related output symbol depends on both the corresponding input symbol and the previous one. This dependency of the output on the past input makes the *channel with memory*. On the other way around, when we focus on the first of the two time slots, the related output symbol depends on both the corresponding input symbol and the next one. This dependency of the output on the future input makes the *channel with anticipation*. Therefore, in modeling the channel, memory and anticipation need to be captured. In Section IV-B, we present the channel model in this case.

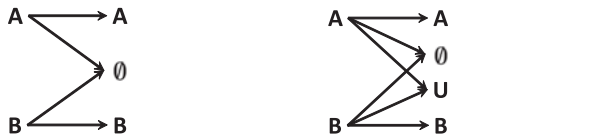

(a) Exposed coalesced droplet ($L_{coal} \geq T_b - T_{SZ}$)

(b) Hidden coalesced droplet ($L_{coal} < T_b - T_{SZ}$)

Fig. 7. Channel model

To discuss the above two cases, in the following we refer to the terminology in Fig. 5, where the time slot is subdivided in several zones which are relevant because the presence of a droplet (coalesced or not) in each zone determines different occurrences to be captured in the model.

In particular, we assume that the coalescence between two droplets occurs in a zone, here referred to as *coalescing zone*, CZ, symmetrically placed at the edge of the two respective time slots. More specifically, for each time slot we consider two coalescing zones of duration $T_{CZ} = \frac{\Delta_C}{2}$, and we refer to the coalescing zone on the side of the previous time slot, as *backward coalescing zone*, CZ_B, and to the coalescing zone on the side of the next time slot, as *forward coalescing zone*, CZ_F.

Depending on the lengths of the sensing and coalescing zones and the time slot, the sensing and the coalescing zones may be disjoint or partially overlapped. In the first case (see Fig. 5(a)), we refer to the zone between the sensing and the coalescing zones as *midway zones* MZ (or *backward* and *forward* midway zones, MZ_B and MZ_F, respectively, to identify the side with respect to the center of the time slot, i.e. towards the previous and the next time slots, respectively).

When, on the contrary, the sensing zone and the coalescing zones overlap, no midway zones exist. It is the case in Fig. 5(b) where the *backward* and *forward overlapped zones*, OZ_B and OZ_F, respectively, are indicated. In the same figure, we refer to the non-overlapping part of the sensing and coalescing zones as $\hat{SZ}$, $\hat{CZ}_B$, and $\hat{CZ}_F$.

The overlapped and midway zones are determined by the length of the droplet with respect to the distance between the sensing and the coalescing zones. More specifically, let L_S be the droplet length. If the distance between the sensing and the coalescing zones is greater than the droplet length L_S, i.e., $L_S < \frac{T_b - T_{SZ} - \Delta_C}{2}$, then we are in the case of Fig. 5(a), where the backward and forward midway zones MZ_B and MZ_F are present. On the contrary, when the distance between sensing and coalescing zones is lower than the droplet length, i.e. $L_S \geq \frac{T_b - T_{SZ} - \Delta_C}{2}$, no midway zones can be found and two overlapped zones, OZ_B and OZ_F, are present (see Fig. 5(b)).

Note that the presence of a droplet inside a coalescing zone is not a sufficient condition for the coalescence to occur. In fact, the coalescence occurs only if the adjacent coalescing zones of two consecutive time slots are both occupied by the corresponding droplets. In the opposite case, we must

This article has been accepted for publication in a future issue of this journal, but has not been fully edited. Content may change prior to final publication. Citation information: DOI 10.1109/TCOMM.2017.2755649, IEEE Transactions on Communications

TABLE I
PROBABILITIES OF A DROPLET INSIDE THE TIME SLOT ZONES

p_{GZ}	d_1	d_2
p_{SZ}	$-\frac{T_{SZ}+L_S}{2}$	$\frac{T_{SZ}+L_S}{2}$
p_{CZ}	$\frac{T_b-\Delta_C-L_S}{2}$	$+\infty$
p_{MZ} *	$\frac{T_{SZ}+L_S}{2}$	$\frac{T_b-\Delta_C-L_S}{2}$
p_{OZ} **	$\frac{T_b-\Delta_C-L_S}{2}$	$\frac{T_{SZ}+L_S}{2}$
$p_{\hat{S}Z}$ **	$-\frac{T_b-\Delta_C-L_S}{2}$	$\frac{T_b-\Delta_C-L_S}{2}$
$p_{\hat{C}Z}$ **	$\frac{T_{SZ}+L_S}{2}$	$+\infty$

* only if $T_{SZ} < T_b - \Delta_C - 2L_S$

** only if $T_{SZ} \geq T_b - \Delta_C - 2L_S$

distinguish between three sub-cases:

1) coalescing and sensing zones are disjoint (Fig. 5(a)): the droplet inside the coalescing zone is not detected;
2) coalescing and sensing zones overlap (Fig. 5(b)) and the droplet is inside the overlapped zone: the droplet is detected;
3) coalescing and sensing zones overlap (Fig. 5(b)) and the droplet is outside the overlapped zone: the droplet is not detected.

In the following, the probability that a droplet is in a generic zone GZ inside the time slot, when it reaches the receiver or when it is involved in a coalescence event, is the probability that the droplet delay D is in the interval (d_1, d_2), that is:

$$p_{GZ} = \wp(D \in (d_1, d_2))) = \int_{d_1}^{d_2} f_D(\theta) d\theta = \int_{\sqrt{2}d_1}^{\sqrt{2}d_2} f_E(\theta) d\theta \quad (1)$$

where the values of d_1 and d_2, for each zone inside the time slot, are summarized in Table I.

According to the position of the droplets inside the time slot, an event that we need to statistically characterize is the coalescence between two consecutive droplets. As said before, the coalescence occurs when two consecutive droplets are both in the coalescing zones between the corresponding time slots. Therefore, the probability of coalescence p_C is given by:

$$p_C = p_{CZ}^2 \quad (2)$$

Note that the probability of coalescence for a single droplet, that we will indicate as p'_C, is the probability that such a given droplet is involved in a coalescence event with anyone of the adjacent droplets. Therefore, we need to consider the two disjoint coalescence events (each of them occurring with probability p_C), between the given droplet and the one in the previous time slot, and between the given droplet and the one in the next time slot. Accordingly,

$$p'_C = 2p_C \quad (3)$$

Another event that we need to statistically characterize is the hidden droplet probability p_H, which is the probability that no droplets are detected inside a time slot. In the case of hidden coalesced droplet (i.e. $L_{coal} < T_b - T_{SZ}$), if sensing and coalescing zones are disjoint then this probability is given by the probability that the droplet moves outside the sensing zone. If sensing and coalescing zones overlap, the droplet is not detected if it moves outside the sensing zone, or if it moves in the overlapped zones and is involved in a coalescence event that produces a hidden coalesced droplet. Instead, in the case of exposed coalesced droplet, i.e. $L_{coal} \geq T_b - T_{SZ}$, the droplet is not detected if it moves outside the sensing zone without coalescing with the adjacent droplet, or in the midway zone, if it exists. Therefore:

$$p_H = \begin{cases} 1 - p_{SZ} & \text{if } T_{SZ} \leq T_b - \Delta_C - 2L_S \\ 2p_{\hat{C}Z} + 2p_{OZ}(p_{OZ} + p_{\hat{C}Z}) & \text{otherwise} \end{cases}$$

and (4)

$$p_H = \begin{cases} 2p_{MZ} + 2p_{CZ}(1 - p_{CZ}) & \text{if } T_{SZ} \leq T_b - \Delta_C - 2L_S \\ 2p_{\hat{C}Z}(1 - p_{OZ} - p_{\hat{C}Z}) & \text{otherwise} \end{cases}$$

when $L_{coal} < T_b - T_{SZ}$ and $L_{coal} \geq T_b - T_{SZ}$, respectively.

A. Channel model in the case of hidden coalesced droplet ($L_{coal} < T_b - T_{SZ}$)

As mentioned before, when a channel error produces coalesced droplets that remain outside the sensing zone ($L_{coal} < T_b - T_{SZ}$), the channel is memoryless. In fact, the output symbol received in a given time slot can be either equal to the transmitted symbol in the same time slot, when no errors occur in this time slot, or to the symbol $\emptyset$, in the case the droplet associated to the time slot moves outside the sensing zone, regardless of whether it coalesces with an adjacent one. In other words, even if the coalescence event involves two droplets belonging to two different time slots, the received output symbol is $\emptyset$, regardless of the symbols associated to the adjacent time slots. So, in this case, the discrete memoryless channel is characterized by the input and output alphabets defined so far as $\mathcal{X} = \{A, B\}$ and $\mathcal{Y} = \{A, B, \emptyset\}$, and a fixed conditional probability, $p_{Y|X}(y|x)$, defined for each symbol x in the input alphabet $\mathcal{X}$ and each symbol y in the output alphabet $\mathcal{Y}$. In order to evaluate the conditional probability $p_{Y|X}(y|x)$, we will evaluate how the input symbol $X = A$ can evolve towards each of the possible output ones. Let us consider all the possible occurrences:

- $A \to A$: if the symbol A is transmitted and received with zero errors, it means that the droplet associated to the transmitted symbol remains inside the sensing zone, in the case $T_{SZ} < T_b - \Delta_C - 2L_S$, and does not coalesce with an adjacent droplet when it is the overlapped zone, in the case $T_{SZ} \geq T_b - \Delta_C - 2L_S$. Note that this probability is complementary to the hidden droplet probability p_H, defined in (4). Therefore, according to (1) and (4), we have:

$$p_{Y|X}(A|A) = \wp(Y = A|X = A) = 1 - p_H \quad (5)$$

- $A \to B$: in the system we are considering, the chemical composition of the droplets is assumed not to change inside the channel (Fig. 7(a)). Therefore, we have:

$$p_{Y|X}(B|A) = \wp(Y = B|X = A) = 0 \quad (6)$$

- $A \to \emptyset$: if the symbol $\emptyset$ is received, it means that no droplets are present inside the sensing zone. The probability $\wp(Y = \emptyset|X = A)$ is the hidden droplet probability p_H:

$$p_{Y|X}(\emptyset|A) = \wp(Y = \emptyset|X = A) = p_H \quad (7)$$

Dual results apply to the case in which the input symbol is $X = B$. Summarizing, the conditional probability $p_{Y|X}(y|x)$ is:

$$p_{Y|X}(y|x) = \begin{cases} 1-p_H & \text{if } x=A, \quad y=A \\ p_H & \text{if } x=A, \quad y=\emptyset \\ 1-p_H & \text{if } x=B, \quad y=B \\ p_H & \text{if } x=B, \quad y=\emptyset \\ 0 & \text{otherwise} \end{cases} \tag{8}$$

B. Channel model in the case of exposed coalesced droplet ($L_{coal} \geq T_b - T_{SZ}$)

When a coalesced droplet is large enough to be sensed in both the sensing zones ($L_{coal} \geq T_b - T_{SZ}$), the coalescence event produces output symbols which depend on the input symbols associated to both the current time slot and one of the adjacent ones. The dependency of the output from the input symbols of the adjacent time slots is not limited to the input history, but is also extended to the future inputs. Therefore, as already said, we need to consider a channel model with memory and anticipation, which is a model that has to capture the dependency of the output symbols from the past and future input symbols. Channels with memory are usually dealt with by using finite-state Markov chains, where the past history of the input symbols is enclosed in the channel state [30], [27], [24]. Applying such approach, in this work we manage the anticipation of the channel, by including future input symbols in the channel state as well.

So, we describe the channel with finite memory and anticipation with an input sequence $\mathbf{x} = \ldots, x_{n+1}, x_n, x_{n-1}, \ldots$[4], an output sequence $\mathbf{y} = \ldots, y_{n+1}, y_n, y_{n-1}, \ldots$, and a state sequence $\mathbf{s} = \ldots, s_{n+1}, s_n, s_{n-1}, \ldots$, where the input and output symbols x_n and y_n are a selection from the alphabets $\mathcal{X} = \{A, B\}$ and $\mathcal{Y} = \{A, B, \emptyset, U\}$, respectively. As far as the channel state is concerned, we define a two-dimensional Markov chain, $\mathbf{S}^{(C)}$, whose generic state in the n-th time slot is s_n. As shown in Fig. 8, the $\mathbf{S}^{(C)}$ state evolution drives the output emission process $\mathbf{Y}$. The state of $\mathbf{S}^{(C)}$ in the generic n-th time slot is defined as $\mathbf{S}^{(C)}(n) = \left(\mathbf{S}^{(Z)}(n), \mathbf{S}^{(R)}(n)\right)$, where $\mathbf{S}^{(Z)}(n)$ represents the movements of three consecutive droplets, and $\mathbf{S}^{(R)}(n)$ represents the three consecutive symbols emitted by the source. More in depth:

- $\mathbf{S}^{(Z)}(n)$ is the state of the Markov chain characterizing the movements of three consecutive droplets associated to the $(n+1)$-th, n-th, and $(n-1)$-th time slots, respectively. Therefore, it is a vector of three elements, i.e. the generic value of $\mathbf{S}^{(Z)}(n)$ is defined as $\mathbf{s}_Z = (z_{\mathcal{N}}, z_C, z_{\mathcal{P}})$, where each element represents the position of the three droplets (associated to the next, current and previous time slots, with respect to the n-th one) inside their own time slot either at the receiver side or immediately before the coalescence with an adjacent droplet occurs[5]. Each element of the vector takes values in the set $\mathcal{Z} = \{SZ, MZ^2, CZ_B, CZ_F\}$ (that is the sensing zone, the union of the backward and forward midway zones, and the backward and forward coalescing zones, respectively, as defined in Section IV), when $T_{SZ} < T_b - \Delta_C - 2L_S$, or in the set $\mathcal{Z} = \{\hat{SZ}, OZ_B, OZ_F, \hat{CZ}_B, \hat{CZ}_F\}$ (that is, the non-overlapped sensing zone, the backward and forward overlapped zones, and the backward and forward coalescing zones, as defined in Section IV), when $T_{SZ} \geq T_b - \Delta_C - 2L_S$. The matrix element $\mathbf{P}^{(Z)}_{[\mathbf{s}_{Z_i}, \mathbf{s}_{Z_j}]}$, representing the conditional probability of entering the state $\mathbf{s}_{Z_j}$, given that the previous state is $\mathbf{s}_{Z_i}$, can be calculated by considering that the movement of a droplet inside its time slot is independent of the movement of the adjacent droplets. Therefore, the probability of a transition from the state $\mathbf{s}_{Z_i}$ in the $(n-1)$-th time slot, to the state $\mathbf{s}_{Z_j}$ in the n-th time slot, is given by:

$$\begin{aligned} \mathbf{P}^{(Z)}_{[\mathbf{s}_{Z_i}, \mathbf{s}_{Z_j}]} &= \mathbf{P}^{(Z)}_{[(z_{\mathcal{N}_i}, z_{\mathcal{C}_i}, z_{\mathcal{P}_i}), (z_{\mathcal{N}_j}, z_{\mathcal{C}_j}, z_{\mathcal{P}_j})]} = \\ &= \begin{cases} \wp(z_{\mathcal{N}_j} = \zeta) & \text{if } z_{\mathcal{C}_j} = z_{\mathcal{N}_i}, \quad z_{\mathcal{P}_j} = z_{\mathcal{C}_i} \\ 0 & \text{otherwise} \end{cases} \end{aligned} \tag{9}$$

where ζ denotes the generic element of $\mathcal{Z}$. The probability $\wp(z_{\mathcal{N}_j} = \zeta)$ that a droplet associated to a given time slot moves into the time slot zone ζ can be calculated as follows:

$$\wp(z_{\mathcal{N}_j} = \zeta) = \begin{cases} p_{SZ} & \text{if } \zeta = SZ \\ 2p_{MZ} & \text{if } \zeta = MZ^2 \\ p_{CZ} & \text{if } \zeta = CZ_B \\ p_{CZ} & \text{if } \zeta = CZ_F \end{cases} \quad \text{and} \quad \wp(z_{\mathcal{N}_j} = \zeta) = \begin{cases} p_{\hat{SZ}} & \text{if } \zeta = \hat{SZ} \\ p_{OZ} & \text{if } \zeta = OZ_B \\ p_{OZ} & \text{if } \zeta = OZ_F \\ p_{\hat{CZ}} & \text{if } \zeta = \hat{CZ}_B \\ p_{\hat{CZ}} & \text{if } \zeta = \hat{CZ}_F \end{cases} \tag{10}$$

when $T_{SZ} < T_b - \Delta_C - 2L_S$ and $T_{SZ} \geq T_b - \Delta_C - 2L_S$, respectively.

- $\mathbf{S}^{(R)}(n)$ is a vector of three elements holding the three consecutive symbols emitted by the source in the $(n+1)$-th, n-th, and $(n-1)$-th time slots, respectively, i.e. $\mathbf{S}^{(R)}(n) = (\mathbf{X}(n+1), \mathbf{X}(n), \mathbf{X}(n-1))$. Therefore, $\mathbf{S}^{(R)}(n)$ represents the state in the n-th time slot of the Markov chain characterizing the *source historical emission process*. The generic value in the n-th time slot is denoted as:

$$\mathbf{s}_{R_n} = (r_{\mathcal{N}}, r_C, r_{\mathcal{P}}) = (x_{n+1}, x_n, x_{n-1}) \tag{11}$$

where $r_{\mathcal{N}}$,r_C, and $r_{\mathcal{P}}$ represent the next, current and previous emitted symbols with respect to the n-th time slot, respectively.

The emission of the input symbols $\mathbf{X}$ is modeled as a stationary discrete Markov process $S^{(X)}$. More specifically, the input symbol $\mathbf{X}(n)$ emitted by the source in the n-th time slot is considered as the state $S^{(X)}(n)$ of the source in that time slot, i.e., $S^{(X)}(n) = \mathbf{X}(n)$. For this reason, in the following we will refer to the process $S^{(X)}$ or $\mathbf{X}$, without distinction. Consistently, we will interchangeably denote the related random variable in the n-th time slot as $S^{(X)}(n)$ or $\mathbf{X}(n)$, and the corresponding values as s_{X_n} or x_n.

[4]Note that, in this paper we will enumerate the sequences of random variables with decreasing indices. This is coherent with the flow direction inside the microfluidic pipes, as depicted in Fig. 5, so that the most recently emitted droplets/symbols appear on the left side with respect to the previously emitted ones.

[5]For the sake of tractability, we have assumed that the coalescence between two droplets may occur in a generic section of the channel, and the new coalesced droplet remains in the middle of two time slots until it reaches the receiver.

This article has been accepted for publication in a future issue of this journal, but has not been fully edited. Content may change prior to final publication. Citation information: DOI 10.1109/TCOMM.2017.2755649, IEEE Transactions on Communications

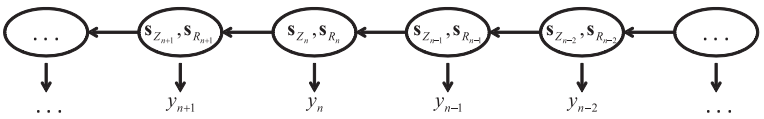

Fig. 8. Channel Markov model

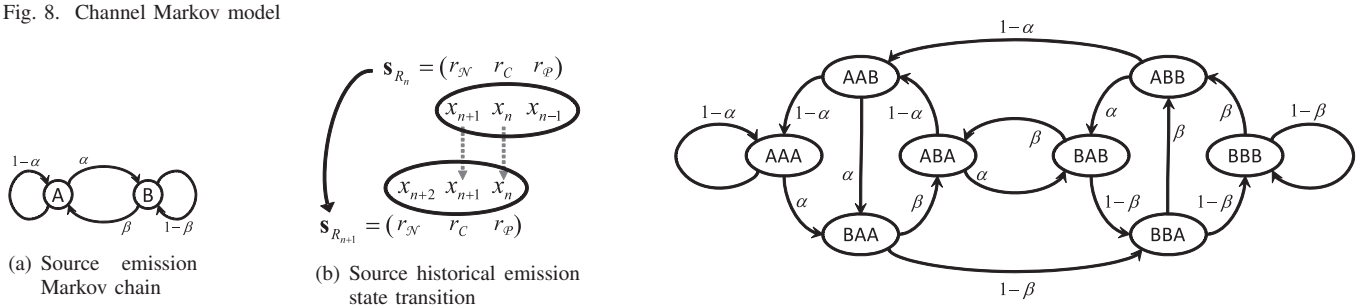

(a) Source emission Markov chain

(b) Source historical emission state transition

(c) Source historical emission Markov chain

Fig. 9. Markov chains describing the source emission process

The source Markov chain $S^{(X)}$, which is depicted in Fig. 9(a), is characterized by the conditional probability $\mathbf{P}^{(X)}_{[s_{X_i},s_{X_j}]}$ of entering the state s_{X_j}, given that the previous state was s_{X_i}, i.e.:

$$\mathbf{P}^{(X)}_{[s_{X_i},s_{X_j}]} = \wp\left(S^{(X)}(n) = s_{X_j} | S^{(X)}(n-1) = s_{X_i}\right) = \\ = \begin{cases} \alpha & \text{if } s_{X_i} = A, \quad s_{X_j} = B \\ 1-\alpha & \text{if } s_{X_i} = A, \quad s_{X_j} = A \\ \beta & \text{if } s_{X_i} = B, \quad s_{X_j} = A \\ 1-\beta & \text{if } s_{X_i} = B, \quad s_{X_j} = B \end{cases} \tag{12}$$

The stationary distribution $\boldsymbol{\pi}^{(X)}$ of the process $S^{(X)}$ can be calculated by solving the linear system $\boldsymbol{\pi}^{(X)}\mathbf{P}^{(X)} = \boldsymbol{\pi}^{(X)}$ with the normalization condition $\sum_{s_{X_i}} \boldsymbol{\pi}^{(X)}_{[s_{X_i}]} = 1$.

Based on the source emission process $S^{(X)}$, we can build the source historical emission Markov chain $\mathbf{S}^{(R)}$, as depicted in Fig. 9(c) using the source historical emission state transitions in Fig. 9(a). It is characterized by the conditional probability $\mathbf{P}^{(R)}_{[\mathbf{s}_{R_i},\mathbf{s}_{R_j}]}$ of entering the state $\mathbf{s}_{R_j}$, given that the previous state was $\mathbf{s}_{R_i}$, which is defined as:

$$\mathbf{P}^{(R)}_{[\mathbf{s}_{R_i},\mathbf{s}_{R_j}]} = \begin{cases} \mathbf{P}^{(X)}_{[r_{\mathcal{N}_i},r_{\mathcal{N}_j}]} & \text{if } r_{\mathcal{C}_j} = r_{\mathcal{N}_i}, \quad r_{\mathcal{P}_j} = r_{\mathcal{C}_i} \\ 0 & \text{otherwise} \end{cases} \tag{13}$$

The two-dimensional Markov chain $\mathbf{S}^{(C)} = \left(\mathbf{S}^{(Z)}, \mathbf{S}^{(R)}\right)$ describing the channel is characterized by the conditional probability $\mathbf{P}^{(C)}_{[\mathbf{s}_{C_{n-1}},\mathbf{s}_{C_n}]}$ of entering the state $\mathbf{s}_{C_n}$, given that the previous state was $\mathbf{s}_{C_{n-1}}$, i.e.:

$$\mathbf{P}^{(C)}_{[\mathbf{s}_{C_{n-1}},\mathbf{s}_{C_n}]} = \wp\left(\begin{array}{l|l} \mathbf{S}^{(Z)}(n) = \mathbf{s}_{Z_n}, & \mathbf{S}^{(Z)}(n-1) = \mathbf{s}_{Z_{n-1}}, \\ \mathbf{S}^{(R)}(n) = \mathbf{s}_{R_n} & \mathbf{S}^{(R)}(n-1) = \mathbf{s}_{R_{n-1}} \end{array} \right) = \\ = \mathbf{P}^{(Z)}_{[\mathbf{s}_{Z_{n-1}},\mathbf{s}_{Z_n}]} \mathbf{P}^{(R)}_{[\mathbf{s}_{R_{n-1}},\mathbf{s}_{R_n}]} \tag{14}$$

while the stationary distribution $\boldsymbol{\pi}^{(C)}$ is obtained by solving the linear system $\boldsymbol{\pi}^{(C)}\mathbf{P}^{(C)} = \boldsymbol{\pi}^{(C)}$ with the normalization condition $\sum_{\mathbf{s}_{C_i}} \boldsymbol{\pi}^{(C)}_{[\mathbf{s}_{C_i}]} = 1$.

The Markov chain $\mathbf{S}^{(C)}$ defined so far allows to describe the output emission process $\mathbf{Y}$, which is driven by the state evolution of $\mathbf{S}^{(C)}$ (see Fig. 8). In particular, the output y_n in the n-th time slot, given the channel state $\mathbf{s}_{C_n}$ in the same time slot, is univocally determined. Therefore, the channel is described by a function $g^{(C,Y)}(\mathbf{s}_{C_n})$ of the channel state which associates to each channel state the corresponding output symbol y_n. The function $g^{(C,Y)}(\mathbf{s}_{C_n})$ can be defined as follows:

$$y_n = g^{(C,Y)}(\mathbf{s}_{C_n}) = g^{(C,Y)}((r_{\mathcal{N}}, r_{\mathcal{C}}, r_{\mathcal{P}}), (z_{\mathcal{N}}, z_{\mathcal{C}}, z_{\mathcal{P}})) = \\ = \begin{cases} r_{\mathcal{C}} & \text{if } z_{\mathcal{C}} = SZ \\ \emptyset & \text{if } z_{\mathcal{C}} = MZ^2 \\ \emptyset & \text{if } z_{\mathcal{C}} = CZ_F, \quad z_{\mathcal{P}} \neq CZ_B \\ r_{\mathcal{C}} & \text{if } z_{\mathcal{C}} = CZ_F, \quad z_{\mathcal{P}} = CZ_B, \quad r_{\mathcal{C}} = r_{\mathcal{P}} \\ U & \text{if } z_{\mathcal{C}} = CZ_F, \quad z_{\mathcal{P}} = CZ_B, \quad r_{\mathcal{C}} \neq r_{\mathcal{P}} \\ \emptyset & \text{if } z_{\mathcal{C}} = CZ_B, \quad z_{\mathcal{N}} \neq CZ_F \\ r_{\mathcal{C}} & \text{if } z_{\mathcal{C}} = CZ_B, \quad z_{\mathcal{N}} = CZ_F, \quad r_{\mathcal{C}} = r_{\mathcal{N}} \\ U & \text{if } z_{\mathcal{C}} = CZ_B, \quad z_{\mathcal{N}} = CZ_F, \quad r_{\mathcal{C}} \neq r_{\mathcal{N}} \end{cases}$$

and

$$y_n = g^{(C,Y)}(\mathbf{s}_{C_n}) = g^{(C,Y)}((r_{\mathcal{N}}, r_{\mathcal{C}}, r_{\mathcal{P}}), (z_{\mathcal{N}}, z_{\mathcal{C}}, z_{\mathcal{P}})) = \\ = \begin{cases} r_{\mathcal{C}} & \text{if } z_{\mathcal{C}} = \hat{S}Z \\ r_{\mathcal{C}} & \text{if } z_{\mathcal{C}} = OZ_F, \quad z_{\mathcal{P}} \neq OZ_B \\ r_{\mathcal{C}} & \text{if } z_{\mathcal{C}} = OZ_F, \quad z_{\mathcal{P}} = OZ_B, \quad r_{\mathcal{C}} = r_{\mathcal{P}} \\ U & \text{if } z_{\mathcal{C}} = OZ_F, \quad z_{\mathcal{P}} = OZ_B, \quad r_{\mathcal{C}} \neq r_{\mathcal{P}} \\ r_{\mathcal{C}} & \text{if } z_{\mathcal{C}} = OZ_B, \quad z_{\mathcal{N}} \neq OZ_F \\ r_{\mathcal{C}} & \text{if } z_{\mathcal{C}} = OZ_B, \quad z_{\mathcal{N}} = OZ_F, \quad r_{\mathcal{C}} = r_{\mathcal{N}} \\ U & \text{if } z_{\mathcal{C}} = OZ_B, \quad z_{\mathcal{N}} = OZ_F, \quad r_{\mathcal{C}} \neq r_{\mathcal{N}} \\ \emptyset & \text{if } z_{\mathcal{C}} = \hat{C}Z_F, \quad z_{\mathcal{P}} \neq \hat{C}Z_B \\ r_{\mathcal{C}} & \text{if } z_{\mathcal{C}} = \hat{C}Z_F, \quad z_{\mathcal{P}} = \hat{C}Z_B, \quad r_{\mathcal{C}} = r_{\mathcal{P}} \\ U & \text{if } z_{\mathcal{C}} = \hat{C}Z_F, \quad z_{\mathcal{P}} = \hat{C}Z_B, \quad r_{\mathcal{C}} \neq r_{\mathcal{P}} \\ \emptyset & \text{if } z_{\mathcal{C}} = \hat{C}Z_B, \quad z_{\mathcal{N}} \neq \hat{C}Z_F \\ r_{\mathcal{C}} & \text{if } z_{\mathcal{C}} = \hat{C}Z_B, \quad z_{\mathcal{N}} = \hat{C}Z_F, \quad r_{\mathcal{C}} = r_{\mathcal{N}} \\ U & \text{if } z_{\mathcal{C}} = \hat{C}Z_B, \quad z_{\mathcal{N}} = \hat{C}Z_F, \quad r_{\mathcal{C}} \neq r_{\mathcal{N}} \end{cases} \tag{15}$$

when $T_{SZ} < T_b - \Delta_C - 2L_S$ and $T_{SZ} \geq T_b - \Delta_C - 2L_S$, respectively.

V. Channel capacity

In Section IV we have seen that in the case where $L_{coal} < T_b - T_{SZ}$, the channel can be modeled as a discrete memoryless channel, whereas in the opposite case we have a discrete channel with finite memory and anticipation. In the following subsections we will calculate the channel capacity for each of the above cases.

A. Channel capacity in the case of hidden coalesced droplet ($L_{coal} < T_b - T_{SZ}$)

As described in Section IV-A, when $L_{coal} < T_b - T_{SZ}$, the channel is memoryless. In this case, the channel capacity is the maximum mutual information I between the transmitted signal X and the received signal Y, taken over all input distributions:

$$C = \max_{p_X(x)} I(X;Y) \tag{16}$$

where we have indicated with $p_X(x)$ the marginal distribution of the input symbol X [11]. The mutual information between X and Y is given by:

$$\begin{aligned} &I(X;Y) = H(Y) - H(Y|X) = \\ &= -\sum_{y\in Y} p_Y(y)\log p_Y(y) + \sum_{x\in X} p_X(x) \sum_{y\in Y} p_{Y|X}(y|x)\log p_{Y|X}(y|x) \end{aligned} \tag{17}$$

where $p_Y(y)$ is the marginal distribution function of the output Y, and $p_{Y|X}(y|x)$ is the conditional distribution function of Y given X[6].

Through (16) and (17), the channel capacity can be evaluated, given the conditional distribution function $p_{Y|X}(y|x)$ defined in Section IV-A. From (8) we can see that the channel is a binary-input, ternary-output channel, with the third output symbol $\emptyset$ (erasure) representing complete loss of information about the input symbol. The crossover probability is equal to zero, while the erasure probability (equal to the hidden droplet probability p_H) is the same for each input symbol. Such a channel model corresponds to the well-known binary erasure channel, whose capacity is:

$$C = 1 - p_H \tag{18}$$

Its maximum is achieved when the input distribution $p_X(x)$ is uniform, i.e., $p_X(A) = p_X(B) = 1/2$.

B. Channel capacity in the case of exposed coalesced droplet ($L_{coal} \geq T_b - T_{SZ}$)

As described in Section IV, when $L_{coal} \geq T_b - T_{SZ}$, the coalescence events involve droplets in adjacent time slots and make the output symbols dependent on past or future inputs. Therefore, the channel has memory and anticipation which are both finite, and limited to one input symbol in the past or in the future. Channels with finite memory and anticipation are a particular case of the more general class of channels with asymptotically decreasing memory and anticipation, for which the information capacity has been well-defined [30], [24]. Moreover, it is easy to verify that the Markov chain $\mathbf{S}^{(C)}$, defined in Section IV-B to model the channel, is irreducible and aperiodic. Therefore, the effects of the initial state wears off with time [9]. As a consequence, the channel belongs to the class of the indecomposable finite-state channels and its capacity is given by:

$$C = \lim_{n\to\infty} \max_{p_{\mathbf{X}^n}(\mathbf{x}^n)} \frac{1}{n} I(\mathbf{X}^n;\mathbf{Y}^n) \tag{19}$$

[6]Since using different bases for the logarithms in (17) results in different units for the information measurements, to simplify the notation, as usual we do not specify the base of the logarithm which in this paper is assumed to be always equal to 2. So we will write $log\cdot$ to mean $log_2\cdot$, and the resulting unit for the channel capacity is bits per channel use.

where the maximum of the mutual information rate is taken over all the input distributions $p_{\mathbf{X}^n}(\mathbf{x}^n)$ on $\mathbf{X}^n$, and where $\mathbf{X}^n = (\mathbf{X}(n), \mathbf{X}(n-1), \ldots, \mathbf{X}(1))$ and $\mathbf{Y}^n = (\mathbf{Y}(n), \mathbf{Y}(n-1), \ldots, \mathbf{Y}(1))$ are the sequences of n random variables representing the emitted and received symbols, respectively. The mutual information in (19) can be calculated as:

$$I(\mathbf{X}^n;\mathbf{Y}^n) = H(\mathbf{X}^n) - H(\mathbf{X}^n|\mathbf{Y}^n) \tag{20}$$

where:

$$\begin{aligned} H(\mathbf{X}^n) &= E\left\{-\log \wp(\mathbf{x}^n)\right\} \\ H(\mathbf{X}^n|\mathbf{Y}^n) &= E\left\{-\log \wp(\mathbf{x}^n|\mathbf{y}^n)\right\} \end{aligned} \tag{21}$$

The entropy $H(\mathbf{G}^n)$ of a sequence of generic random variables $G_n, G_{n-1}, \ldots, G_1$, like the ones in (21), is not easy to evaluate. Additionally, the channel capacity in (19) is defined in terms of long-term behavior, which means we are interested in the entropy rate, i.e. the limit for n approaching infinity of $\frac{1}{n}H(\mathbf{G}^n)$. In general there is not certainty that such a limit exists. However, in [11] it is demonstrated that, when the stochastic process $\mathbf{G}$ is stationary, the above limit exists and defines the entropy rate of $\mathbf{G}$, hereon referred to as $\mathscr{H}(\mathbf{G})$. Moreover, when $\mathbf{G}$ is a stationary Markov chain, the entropy rate can be calculated as:

$$\mathscr{H}(\mathbf{G}) = \lim_{n\to\infty} \frac{1}{n} H(\mathbf{G}^n) = -\sum_{i,j} \boldsymbol{\pi}^{(G)}_{[i]} \mathbf{P}^{(G)}_{[i,j]} \log \mathbf{P}^{(G)}_{[i,j]} \tag{22}$$

where $\boldsymbol{\pi}^{(G)}$ is the stationary distribution, and $\mathbf{P}^{(G)}$ is the transition probability matrix of the Markov chain.

Referring to (20), if the collections of random variables $\mathbf{X}^n$, $\mathbf{Y}^n$, and $(\mathbf{X}^n, \mathbf{Y}^n)$ form Markov chains, the problem can be simplified: in this case we could evaluate $H(\mathbf{X}^n|\mathbf{Y}^n)$ as $H(\mathbf{Y}^n) - H(\mathbf{X}^n, \mathbf{Y}^n)$, and apply (22) to calculate the entropy rates of the processes $\mathbf{X}$, $\mathbf{Y}$ and $(\mathbf{X}, \mathbf{Y})$. For the input process $\mathbf{X}$ this is obviously true, whereas it is not true, in general, for the output process $\mathbf{Y}$ or the joint process $(\mathbf{X}, \mathbf{Y})$. So a natural question to ask is whether they form Markov chains in the particular case under study. Unfortunately, the answer is negative, as demonstrated in [19].

Therefore, while the entropy rate of the process $\mathbf{X}$ can be evaluated through the application of (22), we still need to evaluate the conditional entropy rate of $\mathbf{X}$ given $\mathbf{Y}$, $\mathscr{H}(\mathbf{X}|\mathbf{Y})$. To this purpose, we will proceed through the following steps:

-*Step 1* - We show that the entropy rate $\mathscr{H}(\mathbf{X}|\mathbf{Y})$ cannot be expressed in a closed-form, and its computation is made difficult by the dependency from past output symbols.

-*Step 2* - We simplify the problem by modeling the channel as a cascade of two channels (as depicted in Fig. 10). To this purpose, we define a temporary output alphabet $\mathcal{W}$, and show how to modify the model provided in Section IV-B, accordingly.

-*Step 3* - We demonstrate that, for the channel cascade defined in the previous step, the conditional entropy rates $\mathscr{H}(\mathbf{X}|\mathbf{Y})$ and $\mathscr{H}(\mathbf{X}|\mathbf{W})$ are equal.

-*Step 4* - We provide a closed-form expression of the entropy rate $\mathscr{H}(\mathbf{X}|\mathbf{W})$ to be used for the evaluation of the channel capacity in (19).

We will develop the above steps in the following.

This article has been accepted for publication in a future issue of this journal, but has not been fully edited. Content may change prior to final publication. Citation information: DOI 10.1109/TCOMM.2017.2755649, IEEE Transactions on Communications

Step 1 - Let us first consider that the limit for n approaching infinity of $\frac{1}{n}H(\mathbf{X}^n|\mathbf{Y}^n)$ exists, since the system is stationary [11], so the entropy rate is well-defined. Therefore, we can evaluate:

$$\mathscr{H}(\mathbf{X}|\mathbf{Y}) = \lim_{n\to\infty}\frac{1}{n}H(\mathbf{X}^n|\mathbf{Y}^n) \overset{(a)}{=} \lim_{n\to\infty}\frac{1}{n}\sum_{i=1}^{n}H(X_i|\mathbf{X}^{i-1},\mathbf{Y}^i) = \overset{(b)}{=} \lim_{n\to\infty}H(X_n|\mathbf{X}^{n-1},\mathbf{Y}^n)(\text{when this limit exists}) \tag{23}$$

where:

- (a) follows from the application of the entropy chain rule [11];
- (b) follows from the property of the Cesáro mean [23].

In order to compute the last limit in (23), we now evaluate the probability $\wp(x_n|\mathbf{x}^{n-1},\mathbf{y}^n)$, by considering all the possible values of the output symbol y_n in the n-th time slot, case by case:

- $y_n \in \{A,B\}$: in this case, the knowledge of y_n allows to trace the value of the n-th input symbol as $x_n = y_n$, without ambiguity;
- $y_n = \emptyset$: in this case, the knowledge of y_n does not give information about the value of the input symbol x_n in the same time slot. At the same time, the probability of x_n does not depend on any of the past output symbol or input symbols preceding x_{n-1}, when conditioned by x_{n-1};
- $y_n = U$: in this case, we need to discriminate between two different sub-cases according to the values of the past output symbols $\mathbf{y}^{n-1}$. More specifically, from the knowledge that the output symbol y_n in the n-th time slot is U, we infer that the droplet associated to the same time slot has been involved in a coalescence event, and the two coalescing droplets are of different type. However, we do not know whether the coalescence involves the droplet in the $(n-1)$-th or $(n+1)$-th time slot. We can gather this information from the sequence of past output symbols. Indeed, if $y_{n-1} \neq U$, then the coalescence event producing the output value $y_n = U$ involves the droplets in the n-th and $(n+1)$-th time slots. In this case the probability of x_n depends on the value of x_{n-1}, according to the transition probability matrix $\mathbf{P}^{(X)}$. Conversely, if $y_{n-1} = U$ and $y_{n-2} \neq U$, the coalescence event producing the output values $y_n = y_{n-1} = U$ involves the droplets in the n-th and $(n-1)$-th time slots, and $x_n \neq x_{n-1}$, with probability equal to 1. Similarly, if $y_{n-2} = U$, the odd or even number of consecutive output symbols equal to U determines the probability of x_n, given x_{n-1}.

Therefore, we have:

$$\wp(x_n|\mathbf{x}^{n-1},\mathbf{y}^n) = = \begin{cases} 1 & \text{if } y_n \in \{A,B\},\ x_n = y_n \\ p(x_n|x_{n-1}) & \text{if } y_n = \emptyset \\ p(x_n|x_{n-1}) & \text{if } y_{n-k}^n = U, \quad y_{n-k-1} \neq U,\ k \text{ even} \\ 1 & \text{if } y_{n-k}^n = U, \quad y_{n-k-1} \neq U,\ k \text{ odd},\ x_n \neq x_{n-1} \\ 0 & \text{otherwise} \end{cases} \tag{24}$$

Note that the above probability does not depend on past input symbols preceding x_{n-1}. Conversely, it depends on the sequence of past output symbols. Unfortunately, this property prevents us from evaluating the probability in (24) in closed form since it is necessary to consider all the possible sequences of output symbols $\mathbf{y}^n$. Additionally, note that numerical computation of the entropy $H(X_n|X_{n-1},\mathbf{Y}^n)$ has to be iterated for each n, to find the limit, and the convergence may be arbitrarily slow. Nevertheless, after some manipulation, it is possible to transform the problem in an equivalent one, as we will do in Step 2, so that the entropy rate $\mathscr{H}(\mathbf{X}|\mathbf{Y})$ can be computed rather easily, as we will do in Step 4. ■

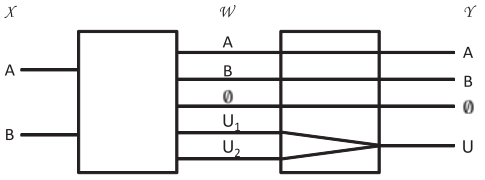

Fig. 10. Cascade of two channels

Step 2 - To simplify the computation of the entropy rate $\mathscr{H}(\mathbf{X}|\mathbf{Y})$, let us note that the dependency of the probability in (24) on past output symbols is essentially due to the fact that the output symbol U always appears in pairs, and we need to discriminate whether it refers to the first or the second occurrence inside the pair (i.e. even or odd position in a sequence of consecutive U output symbols). Therefore, a neat trick we can adopt is to define a temporary output alphabet $\mathcal{W}$, where the odd or even position of each symbol, in a sequence of consecutive U symbols, is identified by U_1 or U_2, respectively. More specifically, we can imagine to have a cascade of two channels (as depicted in Fig. 10), where the alphabet $\mathcal{X}$ is the input of the first channel, the alphabet $\mathcal{W}$ is both the output of the first channel and the input of the second one, and the alphabet $\mathcal{Y}$ is the output of the second channel. Let the alphabet $\mathcal{W} = \{A,B,\emptyset,U_1,U_2\}$ be such that $w_k = y_k$ for $y_k \neq U$, whereas $w_k \in \{U_1,U_2\}$ when $y_k = U$. More specifically, every time two droplets of different type, associated to the $(k+1)$-th and k-th time slots, coalesce in a single one, so producing the sequence $(y_{k+1},y_k) = (U,U)$, we associate to the temporary output symbols w_k and w_{k+1} the values U_1 and U_2, respectively. Note that the model derived in Section IV-B applies to the case the considered output alphabet is $\mathcal{W}$ in place of $\mathcal{Y}$, as long as we replace $g^{(C,Y)}(\mathbf{s}_{C_n})$ with $g^{(C,W)}(\mathbf{s}_{C_n})$. In particular, $g^{(C,W)}(\mathbf{s}_{C_n})$ can be derived from (15) as follows:

$$w_n = g^{(C,W)}(\mathbf{s}_{C_n}) = g^{(C,W)}((r_{\mathcal{N}},r_{\mathcal{C}},r_{\mathcal{P}}),(z_{\mathcal{N}},z_{\mathcal{C}},z_{\mathcal{P}})) = = \begin{cases} U_2 & \text{if } z_{\mathcal{C}} = CZ_F, \quad z_{\mathcal{P}} = CZ_B, \quad r_{\mathcal{C}} \neq r_{\mathcal{P}} \\ U_1 & \text{if } z_{\mathcal{C}} = CZ_B, \quad z_{\mathcal{N}} = CZ_F, \quad r_{\mathcal{C}} \neq r_{\mathcal{N}} \\ g^{(C,Y)}(\mathbf{s}_{C_n}) & \text{otherwise} \end{cases}$$

and

$$w_n = g^{(C,W)}(\mathbf{s}_{C_n}) = g^{(C,W)}((r_{\mathcal{N}},r_{\mathcal{C}},r_{\mathcal{P}}),(z_{\mathcal{N}},z_{\mathcal{C}},z_{\mathcal{P}})) = = \begin{cases} U_2 & \text{if } z_{\mathcal{C}} = OZ_F, \quad z_{\mathcal{P}} = OZ_B, \quad r_{\mathcal{C}} \neq r_{\mathcal{P}} \\ U_1 & \text{if } z_{\mathcal{C}} = OZ_B, \quad z_{\mathcal{N}} = OZ_F, \quad r_{\mathcal{C}} \neq r_{\mathcal{N}} \\ U_2 & \text{if } z_{\mathcal{C}} = \hat{C}Z_F, \quad z_{\mathcal{P}} = \hat{C}Z_B, \quad r_{\mathcal{C}} \neq r_{\mathcal{P}} \\ U_1 & \text{if } z_{\mathcal{C}} = \hat{C}Z_B, \quad z_{\mathcal{N}} = \hat{C}Z_F, \quad r_{\mathcal{C}} \neq r_{\mathcal{N}} \\ g^{(C,Y)}(\mathbf{s}_{C_n}) & \text{otherwise} \end{cases} \tag{25}$$

This article has been accepted for publication in a future issue of this journal, but has not been fully edited. Content may change prior to final publication. Citation information: DOI 10.1109/TCOMM.2017.2755649, IEEE Transactions on Communications

when $T_{SZ} < T_b - \Delta_C - 2L_S$ and $T_{SZ} \geq T_b - \Delta_C - 2L_S$, respectively.

It is easy to verify that the probability in (24) in terms of the temporary output alphabet $\mathcal{W}$ can be rewritten as:

$$\wp(x_n|\mathbf{x}^{n-1},\mathbf{w}^n) = \begin{cases} 1 & \text{if } w_n \in \{A,B\}, \quad x_n = w_n \\ p(x_n|x_{n-1}) & \text{if } w_n = \emptyset \\ p(x_n|x_{n-1}) & \text{if } w_n = U_1 \\ 1 & \text{if } w_n = U_2, \quad x_n \neq x_{n-1} \\ 0 & \text{otherwise} \end{cases} \tag{26}$$

that is, we can write:

$$\wp(x_n|\mathbf{x}^{n-1},\mathbf{w}^n) = \wp(x_n|x_{n-1},w_n) \tag{27}$$

Note that $\wp(x_n|x_{n-1},w_n)$ can be interpreted as a conditional transition probability, from the source state $\mathbf{X}(n-1)$ to the source state $\mathbf{X}(n)$, given $\mathbf{W}(n)$. In the following, it will be denoted as $\mathbf{P}^{(X|W)}_{[(x_{n-1},w_n),x_n]}$, that is:

$$\mathbf{P}^{(X|W)}_{[(x_{n-1},w_n),x_n]} = \wp(x_n|x_{n-1},w_n) \tag{28}$$

■

Step 3 - By modeling the channel as a cascade of two channels, together with the definition of the temporary alphabet $\mathcal{W}$, as done in Step 2, we are able to simplify the computation of the entropy rate $\mathscr{H}(\mathbf{X}|\mathbf{Y})$, since we can demonstrate that

$$I(\mathbf{X}^n,\mathbf{Y}^n) = I(\mathbf{X}^n,\mathbf{W}^n) \tag{29}$$

which implies

$$\mathscr{H}(\mathbf{X}|\mathbf{Y}) = \mathscr{H}(\mathbf{X}|\mathbf{W}) \tag{30}$$

More specifically, in [11] it has been proved that, for a cascade of two channels, we can write:

$$I(\mathbf{X}^n;\mathbf{W}^n) = I(\mathbf{X}^n;\mathbf{Y}^n) + I(\mathbf{X}^n;\mathbf{W}^n|\mathbf{Y}^n) \tag{31}$$

where $I(\mathbf{X}^n;\mathbf{W}^n|\mathbf{Y}^n) = 0$ if and only if, conditional on each $\mathbf{y}^n$, the processes $\mathbf{X}^n$ and $\mathbf{W}^n$ are statistically independent, that is, if:

$$\wp(\mathbf{x}^n,\mathbf{w}^n|\mathbf{y}^n) = \wp(\mathbf{x}^n|\mathbf{y}^n)\wp(\mathbf{w}^n|\mathbf{y}^n) \tag{32}$$

To verify that (32) is true in our case, note that the first term can be rewritten as:

$$\wp(\mathbf{x}^n,\mathbf{w}^n|\mathbf{y}^n) = \wp(\mathbf{x}^n|\mathbf{w}^n,\mathbf{y}^n)\wp(\mathbf{w}^n|\mathbf{y}^n) = \wp(\mathbf{x}^n|\mathbf{y}^n)\wp(\mathbf{w}^n|\mathbf{y}^n) \tag{33}$$

where in the last equality we have removed the dependency on $\mathbf{w}^n$ since $\mathbf{y}^n$ contains the same information as $\mathbf{w}^n$, even if the individual y_n gives less information than w_n. To better explain this property, let us recall that the output alphabets $\mathcal{Y}$ and $\mathcal{W}$ differ only when the coalescence between droplets of different type occurs. More specifically, this event produces a droplet that is detected in two consecutive time slots (let say the $(k+1)$-th and the k-th time slots) and remains unidentified in both of them. This case is represented in the output alphabet $\mathcal{Y}$ by a sequence of two symbols $(y_{k+1},y_k) = (U,U)$, which, according to the definition of the output alphabet $\mathcal{W}$, corresponds to the sequence $(w_{k+1},w_k) = (U_2,U_1)$. Therefore, the single generic symbol w_n holds information about the even or odd occurrence of the symbol U in a sequence of consecutive U output symbols in the output alphabet $\mathcal{Y}$. This means that w_n contains more information than the corresponding y_n. However, when the whole sequence of past symbols $\mathbf{y}^n$ is considered, as in (33), then the count of the number of consecutive U output symbols in the alphabet $\mathcal{Y}$ allows to determine whether the corresponding symbol in the alphabet $\mathcal{W}$ is U_1 or U_2. Therefore, the whole sequences $\mathbf{y}^n$ and $\mathbf{w}^n$ hold the same information. This justify the last equality in (33). ■

Step 4 - Through (30), we are able to compute the entropy rate $\mathscr{H}(\mathbf{X}|\mathbf{Y})$ by replacing $\mathbf{Y}^n$ with $\mathbf{W}^n$ in (23), and then considering (26) and (27). We thus obtain:

$$\mathscr{H}(\mathbf{X}|\mathbf{W}) = \lim_{n\to\infty}\frac{1}{n}H(\mathbf{X}^n|\mathbf{W}^n) = \lim_{n\to\infty}H(X_n|X_{n-1},W_n) = \overset{(a)}{=} \lim_{n\to\infty}H(X_2|X_1,W_2) = H(X_2|X_1,W_2) \tag{34}$$

where (a) follows from stationarity. The last entropy in (23) can be calculated as follows:

$$H(X_n|X_{n-1},W_n) = -\sum_{x_n,x_{n-1},w_n}\wp(x_{n-1},x_n,w_n)\log\wp(x_n|x_{n-1},w_n) =$$
$$= -\sum_{x_n,x_{n-1},w_n}\wp(x_{n-1})\wp(w_n|x_{n-1})\wp(x_n|x_{n-1},w_n)\log\wp(x_n|x_{n-1},w_n) =$$
$$= -\sum_{i,j,k}\boldsymbol{\pi}^{(X)}_{[i]}\boldsymbol{\mu}^{(X,W)}_{[i,k]}\mathbf{P}^{(X|W)}_{[(i,k),j]}\log\mathbf{P}^{(X|W)}_{[(i,k),j]} \tag{35}$$

where $\boldsymbol{\mu}^{(X,W)}$ indicates the conditional probability of $\mathbf{W}(n)$ in the n-th time slot, given $\mathbf{X}(n-1)$ in the $(n-1)$-th time slot. This conditional probability can be calculated as follows:

$$\boldsymbol{\mu}^{(X,W)}_{[x_{n-1},w_n]} = \wp(w_n|x_{n-1}) = \sum_{\mathbf{s}_{C_n}}\wp(w_n|\mathbf{s}_{C_n})\wp(\mathbf{s}_{C_n}|x_{n-1}) \tag{36}$$

where $\wp(w_n|\mathbf{s}_{C_n})$ and $\wp(\mathbf{s}_{C_n}|x_{n-1})$ are given by:

$$\wp(w_n|\mathbf{s}_{C_n}) = \begin{cases} 1 & \text{if } f^{(C,W)}(\mathbf{s}_{C_n}) = w_n \\ 0 & \text{otherwise} \end{cases} \tag{37}$$

and

$$\wp(\mathbf{s}_{C_n}|x_{n-1}) = \wp((r_{\mathcal{N}},r_C,r_{\mathcal{P}}),(z_{\mathcal{N}},z_C,z_{\mathcal{P}})|x_{n-1}) = \begin{cases} \boldsymbol{\pi}^{(C)}_{\mathbf{s}_{C_n}} & \text{if } r_{\mathcal{P}} = x_{n-1} \\ 0 & \text{otherwise} \end{cases} \tag{38}$$

■

Now, the evaluation of the entropy rates $\mathscr{H}(\mathbf{X})$ and $\mathscr{H}(\mathbf{X}|\mathbf{Y})$ through (22) and (34), respectively, allows to calculate the mutual information rate in (19) as:

$$\lim_{n\to\infty}\frac{1}{n}I(\mathbf{X}^n;\mathbf{Y}^n) = \lim_{n\to\infty}\frac{1}{n}I(\mathbf{X}^n;\mathbf{W}^n) =$$
$$= \lim_{n\to\infty}\frac{H(\mathbf{X}^n) - H(\mathbf{X}^n|\mathbf{W}^n)}{n} =$$
$$= -\sum_{i,j}\boldsymbol{\pi}^{(X)}_{[i]}\mathbf{P}^{(X)}_{[i,j]}\log\mathbf{P}^{(X)}_{[i,j]} + \sum_{i,j,k}\boldsymbol{\pi}^{(X)}_{[i]}\boldsymbol{\mu}^{(X,W)}_{[i,k]}\mathbf{P}^{(X|W)}_{[(i,k),j]}\log\mathbf{P}^{(X|W)}_{[(i,k),j]} \tag{39}$$

where the last equality follows from the application of (35) in (34).

Then, we need to find the maximum of the mutual information rate over all the input distributions $p_{\mathbf{X}^n}(\mathbf{x}^n)$. Note that any input distribution is characterized by the probability terms α and β in (12) (see also Fig. 9(a)); so we can express the mutual information rate as a function of α and β, and then evaluate its maximum. To this purpose, by replacing (12), (28) and (36)

This article has been accepted for publication in a future issue of this journal, but has not been fully edited. Content may change prior to final publication. Citation information: DOI 10.1109/TCOMM.2017.2755649, IEEE Transactions on Communications

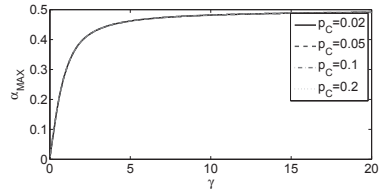

(a) Input symbol distribution that maximizes the mutual information rate

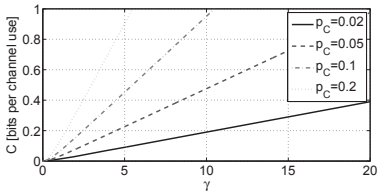

(b) Channel capacity

Fig. 11. Numerical solution of the channel capacity in the case $L_{coal} \geq T_b - T_{SZ}$

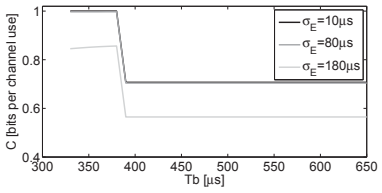

(a) Capacity in bits per channel use

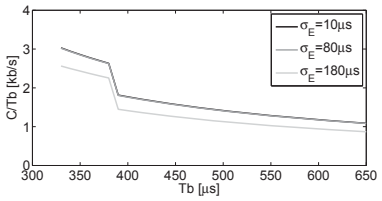

(b) Capacity in kb/s

Fig. 12. Channel capacity in the case $L_{coal} < T_b - T_{SZ}$

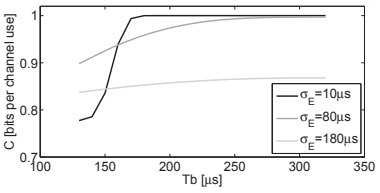

(a) Capacity in bits per channel use

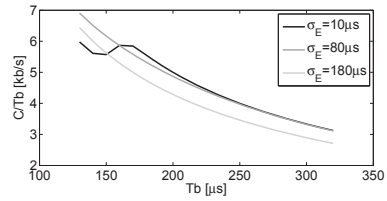

(b) Capacity in kb/s

Fig. 13. Channel capacity in the case $L_{coal} \geq T_b - T_{SZ}$

in (39), it is possible to verify that the mutual information rate can be written as follows:

$$\lim_{n\to\infty} \frac{1}{n} I(\mathbf{X}^n;\mathbf{Y}^n) = \\ = \frac{\beta}{\alpha+\beta}\left(p_C\alpha(1-\alpha+\beta)-(1-p_H)\right)\left(\alpha\log\alpha+(1-\alpha)\log(1-\alpha)\right)+ \\ +\frac{\alpha}{\alpha+\beta}\left(p_C\beta(1-\beta+\alpha)-(1-p_H)\right)\left(\beta\log\beta+(1-\beta)\log(1-\beta)\right) \tag{40}$$

Note that in (40), if α and β are interchanged, the function yields exactly the same results as the original, which means that the mutual information rate is symmetric. This result was expected, since the system does not discriminate between droplets of different types. Therefore, the partial derivatives needed to maximize (40) with respect to α and β are equal, so they are both equal to zero when $\alpha = \beta$. Then, by replacing β with α, we obtain a function of a single variable α, as follows:

$$\lim_{n\to\infty} \frac{1}{n} I(\mathbf{X}^n;\mathbf{Y}^n) = \left(p_C\alpha-(1-p_H)\right)\left(\alpha\log\alpha+(1-\alpha)\log(1-\alpha)\right) \tag{41}$$

In order to find the channel capacity, we need to maximize the function in (41) over α. Unfortunately, this maximum cannot be calculated in closed-form. Nevertheless, its numerical solution is shown in Fig. 11. More specifically, the value of α which maximizes the mutual information rate, denoted as α_{MAX}, is shown in Fig. 11(a), as a function of the ratio γ between $(1-p_H)$ and p_C, i.e. $\gamma = \frac{1-p_H}{p_C}$. The corresponding value of the mutual information rate, which represents the channel capacity, is illustrated in Fig. 11(b) for different values of p_C.

VI. Numerical results

In this section we show how the model derived so far can be used to choose the design parameters for the droplet-based microfluidic system proposed in this paper. To this purpose, let us explicitly observe that in both cases of hidden and exposed coalesced droplet we are now able, from (18) and (19), to evaluate the channel capacity as a function of the probabilities p_C and p_H. In the following, we provide some examples of how estimating the value of p_C and p_H in the specific scenario of interest and calculate the capacity accordingly.

A. Numerical results in the case of hidden coalesced droplet ($L_{coal} < T_b - T_{SZ}$)

In Section V-A, we have seen that, in the case of hidden coalesced droplet, the channel capacity is given by (18). Fig. 12 shows the channel capacity in bits per channel use and in kb/s calculated in this case as a function of the time slot duration T_b, for different values of σ_E. As expected, for values of T_b such that $T_{SZ} < T_b - \Delta_C - 2L_S$, the channel capacity does not depend on the transmission bit rate, which is the inverse of T_b, whereas in the opposite case, it decreases for increasing values of T_b. In fact, when $T_{SZ} < T_b - \Delta_C - 2L_S$, that is when the sensing and the coalescing zones are not overlapped, the hidden droplet probability is given by the probability to find the droplets outside the sensing zone, whose size does not depends on T_b. On the contrary, when the sensing and the coalescing zones partially overlap, an additional contribution to the hidden droplet probability is given by the probability of coalescence inside the sensing zone, since this event produces a coalesced droplet. This additional contribution decreases as T_b increases.

Moreover, Fig. 12 shows that, as expected, increasing values of σ_E, which imply more relevant droplet misplacement with respect to its expected position in the center of the time slot, cause the reduction of the channel capacity.

B. Numerical results in the case of exposed coalesced droplet ($L_{coal} \geq T_b - T_{SZ}$)

In the case of exposed coalesced droplet, the channel capacity, which is defined in (19), cannot be calculated in closed-form. Nevertheless, in Section V-B, the numerical solution has been provided, as shown is Fig. 11, which can be used to evaluate the channel capacity according to the values of γ and p_C in the case of interest.

As an example, in a scenario characterized by the parameter values L_S=100μm, L_{coal}=190μm, Δ_C=60μm, T_{SZ}=130μm, T_b=170μm, σ_E=80μm, through (1), (2) and (4) we derive the following values: p_C=0.1, p_H=0.0019 and γ=9.9. Now, from Fig. 11, we can see that the input probability distribution which

maximizes the mutual information rate is about 0.48, which provides a capacity around 0.45.

Let us note that, unlike the case of $L_{coal} < T_b - T_{SZ}$, the input distribution that maximizes the mutual information is not characterized by $\alpha_{MAX} = 0.5$. In particular, α_{MAX} is lower than 0.5, meaning that the probability to emit, in a given time slot, the same symbol emitted in the previous slot, is higher than the probability to emit a different symbol. Moreover, α_{MAX} decreases when γ decreases, that is when the probability of coalescence increases. The reason is that, when a coalescence event involves two droplets of the same type, the associated input symbols can be decoded through the corresponding output symbols without uncertainty. On the contrary, when droplets of different type coalesce in a single one, there is uncertainty about the emitted input symbols. Therefore, the sequences with equal consecutive symbols are more robust to error, than sequences with alternate symbols. On the other hand, this sort of redundancy reduces the amount of transmitted information. Thus, the input distribution which maximizes the mutual information rate is a tradeoff between the two opposite trends.

Finally, Fig. 13 shows the channel capacity in bits per channel use and kb/s as a function of T_b, for different values of σ_E.

VII. Conclusions

In this paper we have studied a droplet-based microfluidic system for Flow-induced Molecular Communications from an information theoretical perspective. We have shown that the related binary discrete microfluidic channel, in some relevant cases, is characterized by memory and anticipation. According to this channel characterization, we have provided a mathematical model based on a finite-state Markov chain, where the past and future input symbols are included in the channel state. We have evaluated the capacity of the binary droplet-based microfluidic channel and provided a closed-form expression for the mutual information rate.

References

[1] I. F. Akyildiz, J. M. Jornet, and M. Pierobon. Nanonetworks: A new frontier in communications. *Commun. ACM*, 54(11):84–89, Nov. 2011.

[2] D. Arnold and H.-A. Loeliger. On the information rate of binary-input channels with memory. In *Communications, 2001. ICC 2001. IEEE International Conference on*, volume 9, pages 2692–2695 vol.9, 2001.

[3] B. L. Bassler. How bacteria talk to each other: regulation of gene expression by quorum sensing. *Curr. Opin. Microbiol.*, 2(6):582–587, Dec 1999.

[4] A. Bicen and I. Akyildiz. Molecular transport in microfluidic channels for flow-induced molecular communication. In *Communications Workshops (ICC), 2013 IEEE International Conference on*, pages 766–770, June 2013.

[5] A. Bicen and I. Akyildiz. System-theoretic analysis and least-squares design of microfluidic channels for flow-induced molecular communication. *Signal Processing, IEEE Transactions on*, 61(20):5000–5013, Oct 2013.

[6] A. Bicen and I. Akyildiz. Interference modeling and capacity analysis for microfluidic molecular communication channels. *Nanotechnology, IEEE Transactions on*, 14(3):570–579, May 2015.

[7] A. O. Bicen and I. F. Akyildiz. End-to-end propagation noise and memory analysis for molecular communication over microfluidic channels. *IEEE Trans. Communications*, 62(7):2432–2443, 2014.

[8] A. O. Bicen, C. M. Austin, I. F. Akyildiz, and C. R. Forest. Efficient sampling of bacterial signal transduction for detection of pulse-amplitude modulated molecular signals. *IEEE Transactions on Biomedical Circuits and Systems*, 9(4):505–517, August 2015.

[9] P. Billingsley. *Probability and Measure*. Wiley-Interscience, 3 edition, Apr. 1995.

[10] A. Biral and A. Zanella. Introducing purely hydrodynamic networking functionalities into microfluidic systems. *Nano Communication Networks*, 4(4):205 – 215, 2013.

[11] T. M. Cover and J. A. Thomas. *Elements of Information Theory (Wiley Series in Telecommunications and Signal Processing)*. Wiley-Interscience, 2006.

[12] K. D. Danov, D. S. Valkovska, and P. A. Kralchevsky. Hydrodynamic instability and coalescence in trains of emulsion drops or gas bubbles moving through a narrow capillary. *J Colloid Interface Sci*, 267(1):243–258, Nov 2003.

[13] E. De Leo, L. Donvito, L. Galluccio, A. Lombardo, G. Morabito, and L. Zanoli. Communications and switching in microfluidic systems: Pure hydrodynamic control for networking labs-on-a-chip. *Communications, IEEE Transactions on*, 61(11):4663–4677, November 2013.

[14] L. Donvito, L. Galluccio, A. Lombardo, and G. Morabito. μ-net: A network for molecular biology applications in microfluidic chips. *Networking, IEEE/ACM Transactions on*, PP(99):1–1, 2015.

[15] L. Donvito, L. Galluccio, A. Lombardo, G. Morabito, A. Nicolosi, and M. Reno. Experimental validation of a simple, low-cost, t-junction droplet generator fabricated through 3d printing. *Journal of Micromechanics and Microengineering*, 25(3):035013, 2015.

[16] A. Einolghozati, M. Sardari, A. Beirami, and F. Fekri. Capacity of discrete molecular diffusion channels. In *Information Theory Proceedings (ISIT), 2011 IEEE International Symposium on*, pages 723–727, July 2011.

[17] A. Feinstein. On the coding theorem and its converse for finite-memory channels. *Information and Control*, 2(1):25 – 44, 1959.

[18] M. J. Fuerstman, P. Garstecki, and G. M. Whitesides. Coding/decoding and reversibility of droplet trains in microfluidic networks. *Science*, 315(5813):828–832, Feb 2007.

[19] L. Galluccio, A. Lombardo, G. Morabito, S. Palazzo, C. Panarello, and G. Schembra. Technical report 18/2016: Appendix to the paper entitled capacity of a binary droplet-based microfluidic channel with memory and anticipation for flow-induced molecular communications. Technical report, December 2016. Avalilable at http://www.diit.unict.it/users/lgalluccio/trdieei201618.pdf.

[20] T. Glawdel and C. Ren. Global network design for robust operation of microfluidic droplet generators with pressure-driven flow. *Microfluidics and Nanofluidics*, 13(3):469–480, 2012.

[21] A. Goldsmith and P. Varaiya. Capacity, mutual information, and coding for finite-state markov channels. *Information Theory, IEEE Transactions on*, 42(3):868–886, May 1996.

[22] S. Guido and V. Preziosi. Droplet deformation under confined poiseuille flow. *Advances in Colloid and Interface Science*, 161(12):89 – 101, 2010. Physico-chemical and flow behaviour of droplet based systems.

[23] G. H. Hardy. *Divergent Series*. Oxford: Claredon Press, 1949.

[24] Y. Hsieh and P. Yeh. Mathematical foundations for information theory in diffusion-based molecular communications. *CoRR*, abs/1311.4431, 2013.

[25] P. Karlson and M. Luscher. 'Pheromones': a New Term for a Class of Biologically Active Substances. *Nature*, 183(4653):55–56, Jan. 1959.

[26] B. Krishnaswamy, C. Austin, J. Bardill, D. Russakow, G. Holst, B. Hammer, C. Forest, and R. Sivakumar. Time-elapse communication: Bacterial communication on a microfluidic chip. *Communications, IEEE Transactions on*, 61(12):5139–5151, December 2013.

[27] Z. Libo, F. Alajaji, and G. Takahara. A binary communication channel with memory based on a finite queue. *Information Theory, IEEE Transactions on*, 53(8):2815–2840, Aug 2007.

[28] T. Nakano, T. Suda, M. J. Moore, R. Egashira, A. Enomoto, and K. Arima. Molecular Communication for Nanomachines Using Intercellular Calcium Signaling. In *5th IEEE Conference on Nanotechnology, 2005. (IEEE-NANO '05)*, volume 2, pages 478–481, July 2005.

[29] R. Oosterbroek and A. van den Berg. *Lab-on-a-Chip; Miniaturized Systems for (BIO)Chemical Analysis and Synthesis*. Elsevier B.V., Amsterdam, 2003.

[30] E. Pfaffelhuber. Channels with asymptotically decreasing memory and anticipation. *Information Theory, IEEE Transactions on*, 17(4):379–385, Jul 1971.

[31] M. Prakash and N. Gershenfeld. Microfluidic bubble logic. *Science*, 315(5813):832–835, Feb 2007.

[32] R. Raj, N. Mathur, and V. V. Buwa. Numerical Simulations of Liquid-Liquid Flows in Microchannels. *Industrial & Engineering Chemistry Research*, 49(21):10606–10614, 2010.

[33] C. E. Shannon. A mathematical theory of communication. *Bell System Technical Journal*, 27(3):379–423, 1948.

[34] S. Y. Teh, R. Lin, L. H. Hung, and A. P. Lee. Droplet microfluidics. *Lab Chip*, 8(2):198–220, Feb 2008.
[35] C.-G. Yang, Z.-R. Xu, and J.-H. Wang. Manipulation of droplets in microfluidic systems. *TrAC Trends in Analytical Chemistry*, 29(2):141 – 157, 2010.

Laura Galluccio received her Laurea Degree in electrical engineering from the University of Catania, Catania, Italy, in 2001. In March 2005 she got her Ph.D. in electrical, computer and telecommunications Engineering at the same university. Since 2002 she is also at the Italian National Consortium of Telecommunications (CNIT), where she worked as a Research Fellow within the VICOM (Virtual Immersive Communications) and the SATNEX Projects. Since November 2010 she is Assistant Professor at the University of Catania. She serves in the Editorial Boards of Elsevier Ad Hoc Networks Journal and Wiley Wireless Communications and Mobile Computing Journal. Her research interests include unconventional communication networks, software defined networks, and network performance analysis. From May to July 2005 she has been a Visiting Scholar at the COMET Group, Columbia University, NY. She is a member of the Sigmobile, IEEE and ACM N2Women Group. In August and September 2015 she has been a Visiting Professor at Supelec, Paris.

Alfio Lombardo received his degree in electrical engineering from the University of Catania, Italy, in 1983. Until 1987, he acted as consultant at CREI, the center of the Politecnico di Milano for research on computer networks, where he was involved as technical leader in the SEDOS, CTS-WAN/FTAM e COST 11 TER - FDT/ABM CEC projects. In 1988 he joined the University of Catania where he is full professor of Telematics (SSD.: ING-INF/03). From 1996 to 2004 he was there the leader of the University of Catania team in the European ACTS project DOLMEN, in the European IST project VESPER, and in the Italian Ministry for University and Scientific Research (MIUR) projects FIRB - TANGO and COFIN - EURO. In 2005 he founded a company as a research spin off of the Informatics and Telecommunication Department in the University of Catania. From 2005 to 2006 he was the national leader of the PRIN project "Fluid Analytical Models of Autonomic Systems: FAMOUS". From 2007 to 2011 he was responsable of the project "Piano ICT per l'eccellenza nel settore Hi-Tech nel territorio catanese (ICT-E1)" supported by the sicilian regional government; in this context he was the scientific coordinator of the OpenLab laboratory. From 2010 to 2017 he has been the Catania team leader of the CNIT (Consorzio Nazionale Interuniversitario per le Telecomunicazioni) research unit. His research interests include distributed applications, network modeling and analysis, multimedia, green networking, microfluidic networks. He is author of more than 150 papers on these subjects.

Giacomo Morabito received the laurea degree and the PhD in Electrical, Computer and Telecommunications Engineering from the Istituto di Informatica e Telecomunicazioni, University of Catania in 1996 and 2000, respectively. From November 1999 to April 2001, he was with the Broadband and Wireless Networking Laboratory of the Georgia Institute of Technology as a Research Engineer. Since April 2001 he is with the Dipartimento di Ingegneria Elettrica Elettronica e Informatica of the University of Catania where he is currently Associate Professor. His research interests focus on analysis and solutions for wireless networks Internet of Things, and microfluidic networks.

Sergio Palazzo (M92−SM99) received the degree in electrical engineering from the University of Catania, Catania, Italy, in 1977. Since 1987, he has been with the University of Catania, where is now a Professor of Telecommunications Networks. In 1994, he spent the summer at the International Computer Science Institute (ICSI), Berkeley, as a Senior Visitor. In 2003, he was at the University of Canterbury, Christchurch, New Zealand, as a recipient of the Visiting Erskine Fellowship. His current research interests are in modelling, optimization, and control of wireless networks, with applications to cognitive and cooperative networking, SDN, and sensor networks. Prof. Palazzo has been serving on the Technical Program Committee of INFOCOM, the IEEE Conference on Computer Communications, since 1992. He has been the General Chair of some ACM conferences (MobiHoc 2006, MobiOpp 2010), and currently is a member of the MobiHoc Steering Committee. He has also been the TPC Co-Chair of some other conferences, including IFIP Networking 2011, IWCMC 2013, and European Wireless 2014. He also served on the Editorial Board of several journals, including IEEE/ACM Transactions on Networking, IEEE Transactions on Mobile Computing, IEEE Wireless Communications Magazine, Computer Networks, Ad Hoc Networks, and Wireless Communications and Mobile Computing.

Carla Panarello Carla Panarello received the Laurea Degree in Electronics Engineering and the PhD in Computer and Telecommunication Engineering, from the University of Catania, Italy, in 2004 and 2010, respectively. From October 2005 to May 2006, she was involved in a research collaboration with CNR about congestion control and performance optimization in TCP/IP networks. From September to November 2006, she has been a visiting student at the Network Research Lab, Computer Science Department, UCLA, under the guidance of Prof. M. Gerla. From 2010 to 2012, she worked as a Research Fellow with the Italian National Consortium of Telecommunications (CNIT), on green networking within the TREND (Towards Real Energy-efficient Network Design) project. Currently, she is a Post Doctoral Reasearcher at the University of Catania. Her current research interests include quality of service and performance analysis of communication networks, green networking, microfluidics and molecular communications.

Giovanni Schembra is Associate Professor at the University of Catania. From September 1991 to August 1992 he was with the Telecommunications Research Group of the Cefriel of Milan, working on traffic modelling and performance evaluation in broadband networks. He was involved in several national and EU projects. In particular, he worked for the University of Catania in the European project DOLMEN (Service Machine Development for an Open Long-term Mobile and Fixed Network Environment), and has been acting as WP leader in the NoE Newcom. His research interests mainly concern with software defined networks (SDN), network functions virtualization (NFV), traffic modeling, cloud computing and data center management, mobile cloud networks.